# CHAPTER 6

# PERSISTENT SIGNALS IN TWO TRANSVERSE DIMENSIONS

In this chapter, we extend the previous one-dimensional analysis of unmodulated resonance islands presented in Chapter 3 to two transverse dimensions. The obvious disadvantage of the previous methods is that they offer little or no hope of investigating two-dimensional resonance strengths experimentally, as persistent signals are not present when a beam is kicked onto a single coupling or difference resonance. However, if the crossing point of two linearly independent resonances is examined with detuning present in both planes, this chapter shows that one expects to find locally phase-locked motion (and corresponding persistent signals) in both planes created by the interaction of the pair of resonances.

In § 6.1 a dual-resonance N-turn map is derived from the results of previous chapters, and predictions for both the stable fixed points of such a map and the island tunes of linearized motion around these fixed points are presented. These results are compared to particle tracking in the octupole-decapole lattice in § 6.2, where the inadequacy of first-order perturbation theory in predicting small oscillation frequencies for this system is demonstrated. § 6.3 discusses this and other possible methods of measuring two-dimensional resonance strengths, and outlines a possible experiment to observe two-dimensional persistent signals, including realistic requirements on availability of controlled nonlinearities.

## 6.1 THEORETICAL PREDICTIONS

Here we examine the crossing point of a one-dimensional resonance and a two-dimensional resonance. For the sake of simplicity and relevance to the previous chapters, the one-dimensional resonance is assumed to be $5Q_x$, while the two-dimensional resonance is completely general, but specified by $kQ_x + lQ_y$. Sac-

rificing other resonance terms with the assumption that they are either small or average out over future summations via the Dirichlet kernel suppression, we can write a one-turn two-dimensional dual resonance Hamiltonian:

$$\begin{aligned} H_1(\psi_x, J_x, \psi_y, J_y) = & \, 2\pi Q_{x0} J_x + 2\pi Q_{y0} J_y \\ & + \frac{1}{2}\alpha_{xx} J_x^2 + \alpha_{xy} J_x J_y + \frac{1}{2}\alpha_{xy} J_y^2 \\ & + V_{50}(J_x)\ \cos(5\psi_x + \phi_{50}) \\ & + V_{kl}(J_x, J_y)\ \cos(k\psi_x + l\psi_y + \phi_{kl})\ . \end{aligned} \tag{6.1}$$

Here $V_{50}$ and $V_{kl}$ contain the functional dependence of the resonance strengths on the actions $J_x$ and $J_y$, since these dependences cannot be expected to be as simple as the one-dimensional case. Note that the detuning contains a nonlinear coupling term $\alpha_{xy}$, even though the absence of linear coupling is still assumed.

Horizontal motion is expected to be resonant when the horizontal tune is on the $5Q_x$ resonance; for the vertical motion to also fall on the two-dimensional resonance, the net phase advance within the angle dependence of this resonance term must be near some multiple of $2\pi$. This gives the natural base tunes for this investigation:

$$Q_{x0} = \frac{M_x}{5} + \delta_x\ , \qquad\qquad Q_{y0} = \frac{M_y}{l} - \frac{kM_x}{5l} + \delta_y\ , \tag{6.2}$$

where $M_x$ and $M_y$ are integers. Here the $\delta_i$ are again assumed to be small, and motion will approximately repeat itself in the 4-dimensional phase space every $N \equiv 5kl$ turns. (This is the maximum value necessary for repetition; the motion will repeat faster than this if 5 and $kl$ are commensurate.) The actions are invariant to zeroth order, and we can sum over $N$ turns to find the first-order $N$-turn Hamiltonian,

$$\begin{aligned} H_N(\psi_x, J_x, \psi_y, J_y) = & \, 2\pi N\ \delta_x\ J_x + 2\pi N\ \delta_y\ J_y \\ & + \frac{N}{2}\alpha_{xx} J_x^2 + N\alpha_{xy} J_x J_y + \frac{N}{2}\alpha_{yy} J_y^2 \\ & + N\ V_{50}(J_x)\ \cos(5\psi_x + \phi'_{50}) \\ & + N\ V_{kl}(J_x, J_y)\ \cos(k\psi_x + l\psi_y + \phi'_{kl})\ . \end{aligned} \tag{6.3}$$

Here the phases of the nonlinearities have absorbed the shift from the summation: $\phi'_{50} \equiv \phi_{50} + 5\pi(N-1)\delta_x$ and $\phi'_{kl} \equiv \phi_{kl} + \pi k(N-1)\delta_x + \pi l(N-1)\delta_y$.

Equation (6.3) has fixed points akin to the one-dimensional fixed points of the analysis in Chapter 2. These can be found by examining the difference equations of motion generated by this Hamiltonian, and setting them to zero at the fixed points of the map.

$$\Delta\psi_x = 0 \quad \rightarrow \quad 2\pi\delta_x + \alpha_{xx}J_{x,fp} + \alpha_{xy}J_{y,fp} + \vartheta(V) = 0 \ , \tag{6.4a}$$

$$\Delta\psi_y = 0 \quad \rightarrow \quad 2\pi\delta_y + \alpha_{xy}J_{x,fp} + \alpha_{yy}J_{y,fp} + \vartheta(V) = 0 \ , \tag{6.4b}$$

$$\Delta J_x = 0 \quad \rightarrow \quad 5\psi_{x,fp} + \phi'_{50} = 2\pi k_x \ , \tag{6.4c}$$

$$\Delta J_y = 0 \quad \rightarrow \quad k\psi_{x,fp} + l\psi_{y,fp} + \phi'_{kl} = 2\pi k_y \ . \tag{6.4d}$$

Assuming the detuning terms are stronger than the resonance driving terms, as before, Equations (6.4a) and (6.4b) are coupled linear equations for the fixed point actions, and so they can be easily solved to find

$$\begin{pmatrix} J_{x,fp} \\ J_{y,fp} \end{pmatrix} = \frac{2\pi}{\alpha_{xy}^2 - \alpha_{xx}\alpha_{yy}} \begin{pmatrix} \alpha_{yy} & -\alpha_{xy} \\ -\alpha_{xy} & \alpha_{xx} \end{pmatrix} \begin{pmatrix} \delta_x \\ \delta_y \end{pmatrix} \tag{6.5}$$

if they are not degenerate; if they are indeed degenerate, no action fixed points exist. Equations (6.4c) and (6.4d) give the fixed point phases:

$$\begin{aligned} \psi_{x,fp} &= \frac{\pi k_x - \phi'_{50}}{5} \ , \\ \psi_{y,fp} &= \frac{\pi k_y - \phi'_{kl} - k\psi_{x,fp}}{l} \ . \end{aligned} \tag{6.6}$$

Motion around these fixed points can be classified in one of four ways depending on the parity of the integers $k_x$ and $k_y$ — it is either hyperbolically unstable in both oscillation directions, hyperbolic in one direction and elliptically stable in the other, or elliptically stable in both oscillation directions. This last case is the one that interests us here, because phase localization in both planes will result in observable persistent signals in both planes. We choose $k_x$ and $k_y$ even for now,

with the knowledge that other fixed points can be investigated by changing their parity and thus the signs of the resonance strengths $V_{50}$ and/or $V_{kl}$.

Now transform the coordinates to those centered on one of these fixed points, $(\psi_x, J_x, \psi_y, J_y) \rightarrow (\theta_x, I_x, \theta_y, I_y)$, via the uncoupled two-dimensional generating function

$$F(\psi_x, I_x, \psi_y, I_y) = (I_x + J_{x,fp})(\psi_x - \psi_{x,fp}) + (I_y + J_{y,fp})(\psi_y - \psi_{y,fp}) \; . \quad (6.7)$$

Applying this transformation to the $N$-turn Hamiltonian (6.3) and keeping only first order terms in the nonlinear strengths $V_{kl}$ and $\alpha_{ij}$ gives a $N$-turn Hamiltonian that has the form of a pair of coupled pendula:

$$\begin{aligned} H_N = & \frac{N}{2}\alpha_{xx} I_x^2 + N\alpha_{xy} I_x I_y + \frac{N}{2}\alpha_{yy} I_y^2 \\ & + N \; V_{50}(J_{x,fp}) \; \cos(5\theta_x) \\ & + N \; V_{kl}(J_{x,fp}, J_{y,fp}) \; \cos(k\theta_x + l\theta_y) \; . \end{aligned} \quad (6.8)$$

The resonance strengths $V_{50,fp}$ and $V_{kl,fp}$ are evaluated explicitly at the action fixed points $(J_{x,fp}, J_{y,fp})$.

Linearizing the coupled motion given by this Hamiltonian is a tedious but straightforward process. The final result of this linearization gives the motion of the angle variables $(\theta_x, \theta_y)$ as

$$\begin{pmatrix} \ddot{\theta}_x \\ \ddot{\theta}_y \end{pmatrix} = N^2 \begin{pmatrix} M_{11} & M_{12} \\ M_{21} & M_{22} \end{pmatrix} \begin{pmatrix} \theta_x \\ \theta_y \end{pmatrix} \; , \quad (6.9a)$$

where time derivatives are taken with respect to $N$-turn motion, and the individual matrix elements of the coupled motion are

$$\begin{aligned} M_{11} &= 25 \; \alpha_{xx} \; V_{50,fp} + k \; V_{kl,fp} \; (k\alpha_{xx} + l\alpha_{xy}) \\ M_{12} &= l \; V_{kl,fp} \; (k\alpha_{xx} + l\alpha_{xy}) \\ M_{21} &= 25 \; \alpha_{xy} \; V_{50,fp} + k \; V_{kl,fp} \; (k\alpha_{xy} + l\alpha_{yy}) \\ M_{22} &= l \; V_{kl,fp} \; (k\alpha_{xy} + l\alpha_{yy}) \; . \end{aligned} \quad (6.9b)$$

There are two normal mode "island" frequencies of the two coupled oscillators in Equation (6.9). These could be found by diagonalizing the matrix $M$, as could the eigenvectors that represent the normal modes of oscillation. However, since we are primarily concerned with the island frequencies here, we can find those by calculating the eigenvalues of $M$ directly. Note that if either or both of these eigenvalues are negative or imaginary, local motion here is unstable and expansion should proceed around a different fixed point, changing either or both of the signs of the resonance strengths in the N-turn Hamiltonian (6.8).

For completeness, the island tunes corresponding to this motion are

$$[2\pi Q_{\mathrm{I}(1,2)}]^2 = \frac{A_{50}V_{50,fp} + A_{kl}V_{kl,fp}}{2} \pm \frac{\sqrt{(A_{50}V_{50,fp} + A_{kl}V_{kl,fp})^2 - \Delta_l V_{50,fp}V_{kl,fp}}}{2} , \tag{6.10a}$$

where the amplitudes $A_{50}$, $A_{kl}$ and $\Delta_l$ are defined by

$$\begin{aligned} A_{50} &= 25\alpha_{xx} , \\ A_{kl} &= (k^2\alpha_{xx} + 2kl\alpha_{xy} + l^2\alpha_{yy}) , \\ \Delta_l &= 100l^2(\alpha_{xx}\alpha_{yy} - \alpha_{xy}^2) . \end{aligned} \tag{6.10b}$$

Assuming that the resonance strengths $V_{50}$ and $V_{kl}$ are both positive, these island tunes are both positive real if $\Delta_l$ lies within the range

$$0 \le \Delta_l(\text{stable}) \le \frac{(A_{50}V_{50,fp} + A_{kl}V_{kl,fp})^2}{V_{50,fp}V_{kl,fp}} . \tag{6.11}$$

An amazing prediction of Equation (6.11) is that if all detuning strengths scale similarly according to some nonlinearity strength, and the resonance strengths scale similarly according to another nonlinearity strength, then the local stability of this system is independent of both these resonance strengths to first order.

One easily testable scaling of the island tune prediction is that the island tunes should scale as the square root of the nonlinearity strength if the resonances are

driven to first order in that strength. The sum of the squares of the island tunes is also a more easily accessible quantity to test against theory; from Equation (6.10a) this is found to be

$$[2\pi Q_{\mathrm{I},1}]^2 + [2\pi Q_{\mathrm{I},2}]^2 = A_{50} V_{50,fp} + A_{kl} V_{kl,fp} \ , \tag{6.12}$$

which scales as the product of the nonlinear strengths driving the detuning and the resonances.

## 6.2 TRACKING OF TWO-DIMENSIONAL RESONANCE ISLANDS AND PERSISTENT SIGNALS

The question remains as to whether such two-dimensional resonance islands can be observed in a tracking code, and whether the first-order analysis suffices to predict their island tunes and locations in phase space. Using the octupole-decapole model and a program Od2Track, which was written to track this model in both transverse dimensions, two-dimensional detuning parameters $\alpha_{ij}$ are first measured as functions of amplitude in both planes and compared to first-order predictions for the octupoles. A working point must be chosen where the $5Q_x$ resonance and another resonance driven to first order by the decapole cross; this point in the tune plane $(Q_{x0}, Q_{y0})$ should also be free of second-order octupole resonances, since such resonances are not calculated in a first-order analysis. Next, two-dimensional resonance islands are found and their fixed point amplitudes and phases are compared to theoretically predicted values. Island tunes are found for the normal mode oscillations within these resonance islands and compared against both absolutely predicted values and scaling with the decapole strength $\tilde{b}_4$.

From the discussion of the octupole-decapole lattice in Chapter 3 we can write the first-order dependences of the Hamiltonian parameters $\alpha_{ij}$ and $V_{kl}$ on the

| Tracking Parameter | Symbol | Value |
|---|---|---|
| Octupole strengths (each) | $\tilde{b}_3$ | 0.0100 |
| Decapole strength | $\tilde{b}_4$ | 0.0015 |
| Horizontal Tune Offset | $\delta_x$ | 0.0050 |
| Vertical Tune Offset | $\delta_y$ | 0.0050 |
| Horizontal Base Tune | $Q_{x0}$ | 20.6050 |
| Vertical Base Tune | $Q_{y0}$ | 20.6550 |

Table 6.1: Parameters used for two-dimensional persistent signal investigation in the tracking program Od2Track.

lattice parameters listed in Table 6.1 . The detuning is driven by the octupoles,

$$\alpha_{xx} = \alpha_{yy} = -\frac{1}{2}\alpha_{xy} = \frac{9}{4}\tilde{b}_3 \tag{6.13a}$$

and the resonances are driven by the decapole:

$$\begin{aligned} V_{50} &= \frac{\sqrt{2}}{20}\tilde{b}_4 J_x^{5/2} \ , \\ V_{1\pm2} &= \frac{\sqrt{2}}{2}\tilde{b}_4 J_x^{1/2} J_y(2J_y - 3J_x) \ , \\ V_{3\pm2} &= -\frac{\sqrt{2}}{2}\tilde{b}_4 J_x^{3/2} J_y \ , \\ V_{1\pm4} &= \frac{\sqrt{2}}{4}\tilde{b}_4 J_x^{1/2} J_y^2 \ . \end{aligned} \tag{6.13b}$$

These detuning parameters give the action dependences of the tunes:

$$\begin{pmatrix} Q_x \\ Q_y \end{pmatrix} = \begin{pmatrix} Q_{x0} \\ Q_{y0} \end{pmatrix} + \frac{9\tilde{b}_3}{8\pi}\begin{pmatrix} 1 & -2 \\ -2 & 1 \end{pmatrix}\begin{pmatrix} J_x \\ J_y \end{pmatrix} \tag{6.14}$$

The resulting "footprint" of this tune shift on the tune plane is a rhombus with an oblique opening angle of 143°; this is shown in Figure (6.1) as contours of constant amplitude. Circles in this figure are tunes for tracked particles, with actions in each plane ranging from 0.0 to 4.0 in steps of 0.4 ; excellent agreement is shown for the situation where particles are not affected by nearby strong resonances. Note that the decapole was not turned off for this check, since the second-order tuneshift from the decapole is expected to be small compared to that of the octupoles.

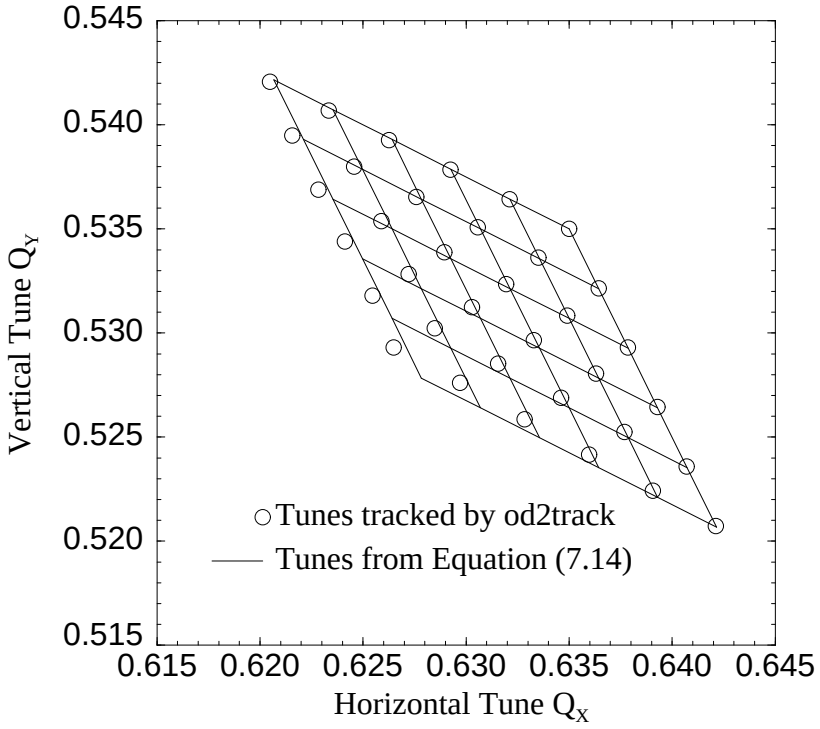


Figure 6.1: Comparison of octupole detuning as predicted by Equation (6.14) to tracking of the octupole-decapole lattice. Lines are predicted contours of constant action, ranging from 0 to 2 in steps of 0.2. Circles represent tracked tune offsets. Magnet strengths are as in Table (6.1); base tunes are $Q_{x0} = 20.66$, $Q_{y0} = 20.64$, far from prevailing resonances.

Now the tune plane must be investigated for an optimal working point for this tracking experiment to find 2-dimensional persistent signals. For agreement with the previous theory, the resonances under investigation should both be driven to first order in the decapole strength, and one should be the horizontal resonance $5Q_x$. Since the octupoles are much stronger than the decapoles in this simulation, creating strong stabilizing detuning, all resonances up to second order in octupole strengths should be avoided. Examination of the tune plane of Figure (6.2), with first order decapole resonances represented by solid lines and second order octupole resonances represented by dashed lines, shows a promising working point at the

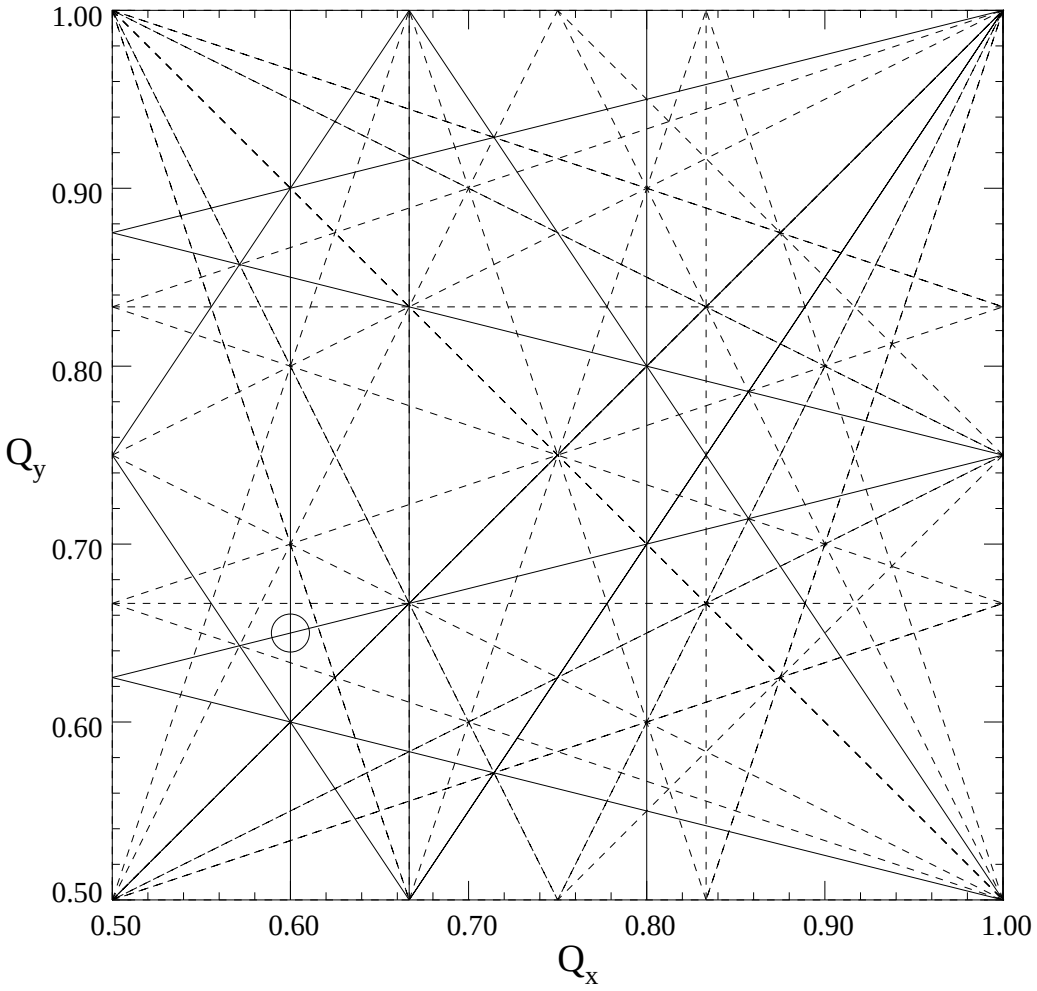


Figure 6.2: The tune plane for the octupole-decapole lattice. Resonances driven to first order in the decapole strength are represented by solid lines; resonances driven to second order in the octupole strength are represented by dashed lines. The circle marks the chosen resonant point, $(Q_{x,res}, Q_{y,res}) = (20.60, 20.65)$, for a 2-dimensional decapole resonance crossing simulation.

resonant tunes

$$Q_{x,res} = 0.600 = \frac{3}{5} , \qquad Q_{y,res} = 0.650 = \frac{13}{20} .$$

At this point the $5Q_x$ and $Q_x - 4Q_y$ resonances cross, so $k = 1$ and $l = -4$. Since both resonance tune denominators are commensurate it suffices to take a Poincaré surface of section every 20 turns, instead of every 100 turns as would be suggested by the previous discussion.

For the tracking conditions of Table (6.1) and previously calculated detuning coefficients, the fixed-point actions are predicted by Equation (6.5) to be $J_{x,fp}(\text{theory}) = J_{y,fp}(\text{theory}) = 1.396$. Instead of going through tedious calculations necessary to predict the fixed point phases, these actions were used as initial conditions with which to track at a variety of initial phases, searching for initial conditions that at least lay within the separatrix of the four-dimensional phase space resonance islands. Such a set of phases, $(\psi_x = 0.2, \psi_y = 0.3)$, was easily found after a small range of initial phases were checked, since the long-term tunes of resonantly trapped particles will be exactly the resonant tunes.

A turn-by turn Poincaré plot of the four-dimensional phase space motion of this set of initial conditions is pictured at the top of Figure (6.3). This plot certainly shows that there is some sort of phase space structure present, but it is difficult to determine whether or not there is resonant motion. Various types of other tools can be used to visualize different sections of this phase space, including three-dimensional projections instead of the two-dimensional projections that are normally used (Holt et. al. 1992). For this analysis, however, a simpler technique is available, which consists of taking a Poincare surface of section every $N = 20$ turns of the motion. If the motion is truly resonant, then this stroboscopic view will show phase-locked motion, and a persistent signal would be visible for a real distribution of particles launched on and near this orbit. This is indeed the case

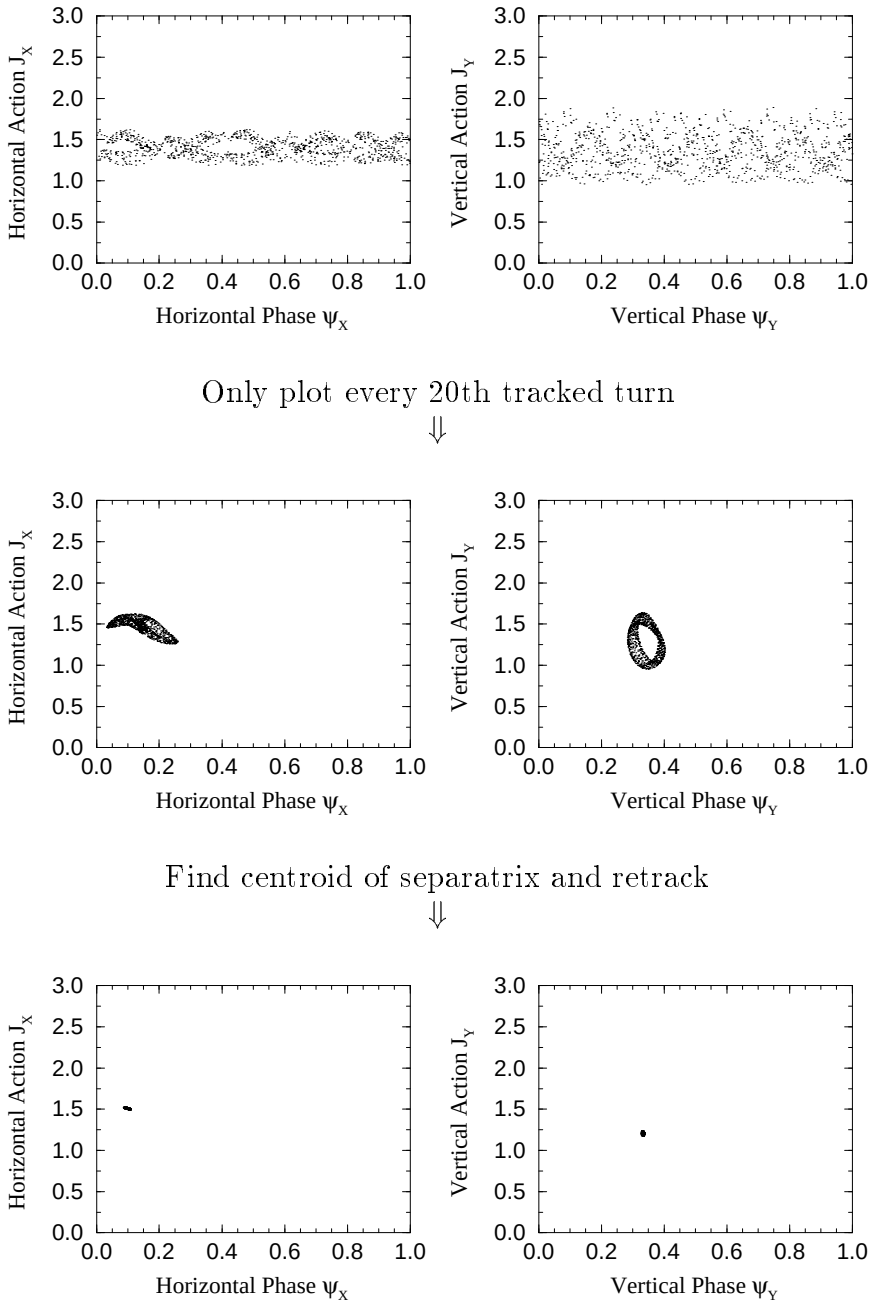


Figure 6.3: Four-dimensional phase space projections used in finding two-dimensional resonance islands and persistent signals. Coherent motion is evident in all three plots.

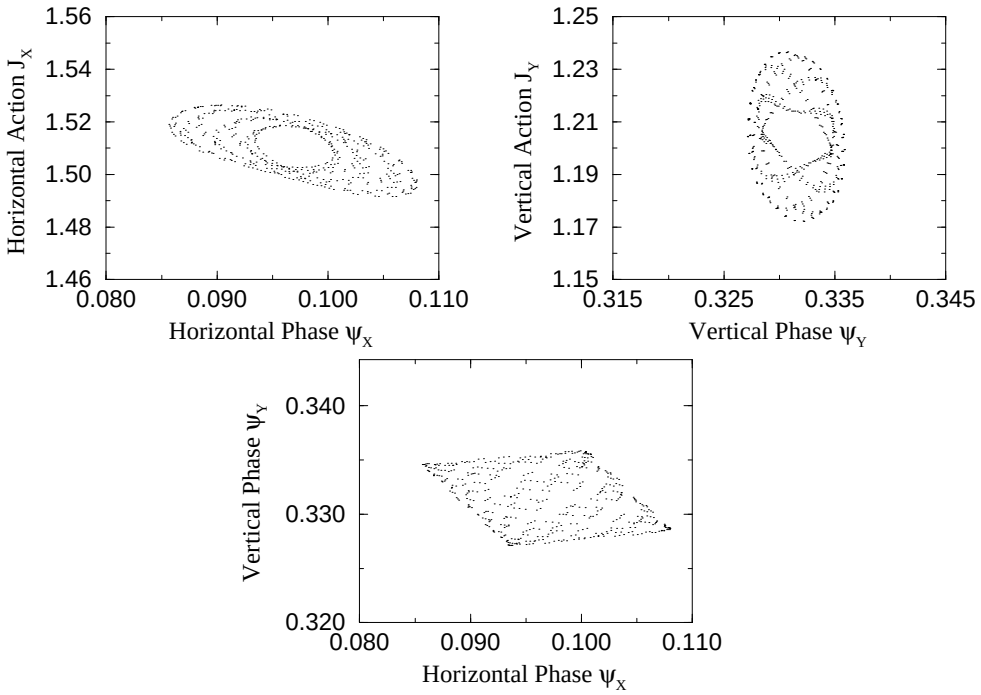


Figure 6.4: Close-up of tracking very near the fixed point of the two-dimensional resonance islands, plotted every 20th turn.

for the above initial conditions, as can be seen in the middle of Figure (6.3) — a resonant orbit appears.

Once any sort of resonant orbit has been found, an iterative process can be used to find the actual fixed point of the lattice used for tracking. The centroid of the distribution in each plane is calculated for a number of turns much larger than the expected island periods, thus averaging over many rotations in the island, and these centroids are substituted back into the tracking program as new initial coordinates. This is much less efficient than the more sophisticated methods used in the one-dimensional fixed-point location algorithm of Chapter 4, but is much more easily implemented than would be the corresponding 2-dimensional extension of such an approach. Four iterations yield the fixed point of the lattice

described in Table (6.1) to four significant figures,

$$(\psi_{x,fp}, J_{x,fp}) = (0.0967, 1.5104) ,$$

$$(\psi_{y,fp}, J_{y,fp}) = (0.3314, 1.2040) ,$$

which is gives modest (10-15%) agreement with the fixed point amplitudes predicted by theory. The resulting phase space of an intermediate step of this iterative process is shown at the bottom of Figure (6.3), and magnified in Figure (6.4) to show the character of motion for small amplitudes $I_i$ near the fixed point. This motion falls on a two-dimensional torus embedded in the four-dimensional phase space, since there are two invariants corresponding to the locally phase-locked motion in each transverse dimension.

Once the fixed point has been found, the island tunes can be measured from tracking data by taking 20-turn stroboscopic data from either plane and performing an FFT on some portion of data with $2^n$ data points. Taking 16384 data points suffices for a measurement of these tunes to an accuracy of approximately $10^{-4}$, and gives $Q_{I,1} = 2.1 \cdot 10^{-4}$ and $Q_{I,2} = 8.7 \cdot 10^{-4}$ for the data presented in Figure (6.4).

For a large range of decapole strengths, up to strengths comparable to the octupole strength, the island tunes are displayed in Figure (6.5). One peak from the FFT of small oscillatory motion scales according to $\tilde{b}_4^{1/2}$ as predicted, but the other appears to scale linearly. No other significant peaks appear in an examination of the FFT of this motion, indicating that the linear scaling is not an anomolous peak created by interference of the natural oscillation frequencies. There is also no evidence that these peaks are aliased from higher frequencies, as they each approach zero at zero decapole strengths.

The island tunes predicted by Equations (6.10a) and (6.10b) are also shown in Figure (6.5), and are nearly three to five times larger than the island tunes found by tracking. The inconsistency between theory and tracking for the resonant

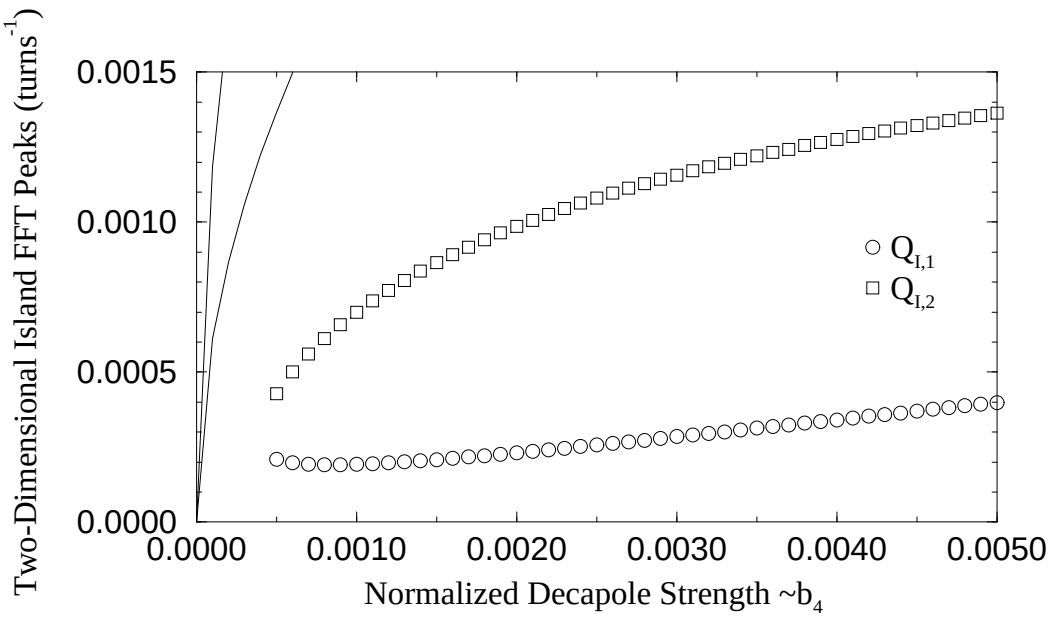


Figure 6.5: Two-dimensional island tunes $(Q_{I,1}, Q_{I,2})$ measured as a function of decapole strength $\tilde{b}_4$ in the tracking program Od2fp. All other lattice parameters for this tracking are as listed in Table (6.1). Lines are theoretical predictions for island tunes.

crossing point small oscillation tunes also appears at other values of the octupole strength as well as other resonance crossing points where second-order octupole resonances are present. This inability of first-order perturbation theory to predict the small-oscillation motion in these areas of the tune plane is a strong indication that such approaches fail to give meaningful results at the crossing of several resonances. Higher order resonances are undoubtedly present at these crossing points, and possibly higher orders of perturbative magnet strengths must be introduced to reconcile theory with tracking. However, with the addition of other resonances the linearization process previously described becomes difficult, particularly because the equations defining the fixed-point phases are transcendental.

## 6.3 A POSSIBLE EXPERIMENT

How might these two-dimensional persistent signals be observed in a real accel-

erator? First, one must operate with a small beam — much smaller, in fact, than any available at the Fermilab Tevatron, since the Tevatron beam size is typically one-tenth of the physical aperture. Use of a small cooled beam would be optimal, since this would maximize the proportion of the beam actually trapped within the four-dimensional phase space well and produce the highest signal-to-noise ratio for persistent signals in both planes.

Kicks to move the beam onto the two-dimensional resonance islands cannot be applied independently in each plane with linear coupling present; such linear coupling would rapidly transfer energy in the kicked plane to energy in the unkicked plane, increasing the beam emittance in the unkicked dimension. Linear coupling can be removed globally by adjustment of skew quadrupoles, a standard procedure that was also performed in E778 for the explicitly horizontal one-dimensional kick.

The lattice must be studied extensively for nonlinearities before the study is begun, and both linear and nonlinear coupling must be removed as much as possible. This implies measuring the detuning coefficients $\alpha_{xx}$, $\alpha_{yy}$, and $\alpha_{xy}$. The nonlinear coupling $\alpha_{xy}$ can be measured by kicking the beam in one transverse plane and observing the tune shift in the unkicked plane, far from strong resonances. Measurement of three or four points should suffice for a reasonable measurement, and then octupoles (if present) can be adjusted to remove this component. When the nonlinear coupling has been removed, turn-by-turn data can be taken in both planes with separate kicks to test the turn-by-turn data acquisition system and measure the detuning coefficients $\alpha_{xx}$ and $\alpha_{yy}$, as has been done previously in E778.

Once the detuning coefficients are known, the actual amplitudes of the resonance islands can be calculated to first order, and base tunes can be chosen to optimize the positions of the four-dimensional phase space fixed points. Kicking first in the

plane where the one-dimensional resonance is present, a systematic scan of various kick amplitudes can be performed, and persistent signals should be evident when the beam is kicked onto the one-dimensional resonance island. Up to this point such an experiment reproduces previous persistent signal results of E778 without tune modulation, as well as those of Experiment CE22 at IUCF.

Once the kick amplitude has been found which consistently populates the one-dimensional resonance island, another kick in the opposite plane can be inserted in the cycle after the first kick. If linear and nonlinear coupling have been sufficiently minimized this kick does not couple into motion in the opposite the plane which has already been resonantly captured, and so it does not disturb this motion. A similar scan of various kick amplitudes can then be performed in this plane, searching for production of another persistent signal.

For the purposes of practical measurement of the strengths of two-dimensional resonances this method is most probably inadequate, since the crossing points where two-dimensional persistent signals are present are also crossed by many other resonances which affect the motion around the fixed point. This is evident in the failure of first-order perturbation theory to predict island tunes. Other techniques involving observation of orbit distortions in four-dimensional phase space have been investigated, and prove to be more promising for this application (Li 1990, Liu 1989). However, such an experiment could be considered a prelude to investigations of modulational diffusion, which provides a mechanism for luminosity and luminosity lifetime limitations in storage rings as described in the next chapter. Modulational diffusion is expected to be present near the intersection of two strong resonances, in the same region of the tune plane that two-dimensional persistent signals could be observed.